Sensors and Actuators B 255 (2018) 1211–1219

Contents lists available at ScienceDirect

Sensors and Actuators B: Chemical

journal homepage: www.elsevier.com/locate/snb

Hydrothermal synthesis of Ce-doped hierarchical flower-like In_2O_3 microspheres and their excellent gas-sensing properties

Dongdong Wei[b], Zhangshu Huang[b], Liwei Wang[b], Xiaohong Chuai[a,b,*], Sumei Zhang[b], Geyu Lu[a,b,*]

[a] State Key Laboratory of Automotive Simulation and Control, Jilin University, 5988 Renmin Street, Changchun 130012, People's Republic of China
[b] State Key Laboratory on Integrated Optoelectronics, College of Electronic Science and Engineering, Jilin University, 2699 Qianjin Street, Changchun, 130012, People's Republic of China

ARTICLE INFO

Article history:
Received 19 April 2017
Received in revised form 22 June 2017
Accepted 22 July 2017
Available online 24 July 2017

Keywords:
Ce-doped In_2O_3
Hydrothermal
Hierarchical structures
Acetone sensor

ABSTRACT

Pure and 1–5 mol% Ce-doped hierarchical flower-like In_2O_3 microspheres with uniform sizes were synthesized via environment friendly one-step hydrothermal method. Their phase structures, morphologies properties and element composition were investigated by different kinds of techniques, including X-ray diffraction (XRD), field-emission scanning electron microscopy (FESEM), transmission electron microscopy (TEM), high-resolution transmission electron microscopy (HRTEM) and X-ray photoelectric spectroscopy (XPS). Their gas-sensing properties were tests for several kinds of Volatile Organic Compounds (VOCs). The results indicated that Ce doping could greatly improve sensing performances of In_2O_3 gas sensors. Among all the samples (0, 1, 3 and 5 mol% Ce-doped In_2O_3), 3 mol% Ce-doped In_2O_3 exhibited the highest response toward 200 ppm acetone at 250 °C, having a response of 41.8, which was about 4 times higher than pure In_2O_3. Furthermore, good repeatability and long term stability were achieved, showing its prospect for excellent acetone gas sensor with high performance.

1. Introduction

With the increasing attention on environmental protection and citizen security, gas sensors with excellent performance are becoming necessary. The occurrence of accidents or disasters could be effectively prevented by detecting toxic and harmful, especially those flammable and explosive gases [1–6]. So far, several kinds of gas sensors have been studied based on different sensing materials. Among the sensors, the resistance-type gas sensors which adopt metal oxide semiconductors (MOS) as gas sensing materials hold a vital position due to their advantages of low cost, high sensitivity, and simplicity of operation. The metal oxide semiconductors, including In_2O_3 [7,8], ZnO [9,10], SnO_2 [11,12], NiO [13,14], Fe_2O_3 [15,16] and WO_3 [17,18] have been widely investigated in the past few decades. Among them, Indium oxide (In_2O_3), an *n*-type direct band semiconductor (E_g = 2.8 eV), has been acknowledged as a promising candidate for practical gas sensing application due to its high conductivity and abundant defects both in the sensing body and on the surface [19–21].

As is well known, the reaction between the adsorbed oxygens and the test gas moleculars on the surface of oxides can account for the resistance change of the semiconductor oxide. Morphology of sensing materials have an effect on surface active sites, surface energy, band structure and gas diffusion, being an important factor in improving the gas sensor properties [22]. Until now, In_2O_3 nanostructures with various morphologies, such as nanoparticals [23], nanowires [24], nanorods [25], nanosheets [26] and nanospheres [27,28], have been fabricated with several physical and chemical methods [29–35]. Among them, hierarchical flower-like microspheres synthesized by one step hydrothermal method have been demonstrated to have great potential in the application of gas sensor due to their large surface-to-volume ratio, good surface permeability, and high interfacial charge-transfer efficiency [36,37].

Doping is also an effective approach to improve the gas sensing performances. Rare-earth and transition metal oxides, have been considered as effective dopants to improve gas-sensing properties of semiconductor materials [38]. For example, Zhao et al. studied the response to 1 ppm nitrogen dioxide gas could be enhanced up to 4 times via Fe-doped mesoporous In_2O_3 gas sensor [39]. Hu et al. investigated the gas-sensing characteristics of Cu doping for In_2O_3 hierarchical flowers, with a marked improvement for 400–1800 ppb nitrogen dioxide [40]. In particular, CeO_2, as a dopant, could enhance gas-sensing properties by its outgoing

* Corresponding authors at: State Key Laboratory on Integrated Optoelectronics, College of Electronic Science and Engineering, Jilin University, 2699 Qianjin Street, Changchun, 130012, People's Republic of China.
E-mail addresses: xhchuai@jlu.edu.cn (X. Chuai), lugy@jlu.edu.cn (G. Lu).

http://dx.doi.org/10.1016/j.snb.2017.07.162
0925-4005/

oxygen storage capacity, rich oxygen vacancies, mending the morphology, changing energy band structure and creating more active adsorption sites [41,42]. Jiang et al. presented the properties of Ce-doped SnO_2 thin films, which have good selectivity for butanone [43]. To the best of our knowledge, there are few reports on acetone-sensing properties of Ce-doped In_2O_3 microspheres.

In this paper, we systemically investigate the synthesis of Ce-doped (0, 1, 3 and 5 mol% Ce) hierarchical flower-like In_2O_3 microspheres via one-step hydrothermal method and their gas sensor properties. The results indicate that Ce doping can improve the performance of In_2O_3 sensor. 3 mol% Ce-doped In_2O_3 microspheres show excellent gas sensing response towards acetone at 250 °C in comparison with pure In_2O_3 microspheres. Meanwhile, the Ce doped sensor exhibited a good repeatability and long term stability. The gas sensing mechanism will be elucidated in the following sections.

2. Experimental

2.1. Preparation of pure and Ce-doped hierarchical flower-like In_2O_3 microspheres

All of the chemical reagents involved in the experiment were analytical grade used as received without further purification. Purchased from Sinopharm Chemical Reagent Co. Ltd. $InCl_3{\cdot}4H_2O$ and $Ce(NO_3)_2{\cdot}6H_2O$ were used as indium and Cerium sources, respectively.

In a typical experiment process, 0.13 g (0.45 mmol) of $InCl_3{\cdot}4H_2O$, a certain amount of $Ce(NO_3)_3{\cdot}6H_2O$ (in a ratio of 1, 3 and 5 mol% respectively), 1.00 g of urea and 0.13 g of sodium dodecyl sulfate (SDS) were added to 40 mL water under vigorous magnetically stirring for 60 min. Then, the homogeneous and transparent solution was transferred into a Teflon-lined stainless-steel autoclave, tightly sealed and maintained at 160 °C for 3 h. After being cooled to room temperature naturally, the white precipitates were collected and washed by centrifugation with distilled water and absolute alcohol for several times. The final products were obtained after sintering the white powders at 500 °C for 2 h.

2.2. Characterization

The X-ray diffraction (XRD) patterns were recorded on a Rigaku TTRIII X-ray diffractometer operated at 40 kV and 200 mA using Cu K radiation with a wavelength of 1.5406 Å. The field emission scanning electron microscopy (FESEM) images were obtained using a JSM-7500F (JEOL) microscope with an operating voltage of 15 kV. Transmission electron microscopy (TEM) and high-resolution transmission electron microscopy (HRTEM), as well as selected-area electron diffraction (SAED) patterns were recorded on a JEM-2200FS instrument (JEOL) at an accelerating voltage of 200 kV. The energy dispersive X-ray spectroscopic (EDS) elemental mapping was investigated by the TEM attachment. X-ray photoelectron spectroscopy (XPS) experiments were recorded on an ESCAlab 250 Analytical XPL Spectrometer with a monochromatic Al Kα source.

2.3. Fabrication and measurement of gas sensor

The schematic of the fabricated gas sensor is shown in Fig. 1. Its fabrication process was as follows: the as-prepared powder was mixed with the deionized water to make a paste, then the paste was coated onto an alumina tube (4 mm in length, 1.2 mm in external diameter, and 0.8 mm in internal diameter, attached with a pair of gold electrodes) to form a thick film. A Ni-Cr alloy coil served as a heater, was inserted into the alumina tube, enabling us to control the operating temperature of the sensor by adjusting the heating current. The detailed fabrication process was described in our previous literature [44]. The gas sensing properties of the sensors were measured by a static test system. First of all, the gas sensors were placed in an airtight chamber purged with fresh air. Then a certain volume of target gases was injected into the airtight chamber by a micro injector in order to measure the sensing performance. When the response run up to a constant value, the upper cover of the test chamber was removed and the sensor began to recover in air. For an oxidizing gas, the response of the sensor is defined as $S = R_g/R_a$. For a reducing gas, the response was defined as $S = R_a/R_g$. R_a and R_g are the resistances of the sensor in air and target gas, respectively. The response and recovery times are defined as the time taken by the sensor to achieve 90% of the total resistance change in the case of adsorption and desorption, respectively.

3. Results and discussion

3.1. Structural and morphological characteristics

The XRD patterns of the as-synthesized undoped and Ce-doped In_2O_3 samples are shown in Fig. 2. All of the diffraction peaks can be indexed to cubic ferromanganese structure of In_2O_3 (JCPDS 65–3170). No other peak corresponding to ceria or cerium compound was observed in the XRD patterns of the doped nanomaterials. Besides, the diffraction peaks became broader with increasing the Ce doping amount. The Scherrer formula $D = 0.89\lambda/\beta\cos\theta$ is used to calculate the average crystallite size of the samples, in which λ is the X-ray wavelength (0.154056 nm), β is the peak width at half maximum, and θ is the Bragg diffraction angle. The calculated values of 0%, 1 mol%, 3 mol%, 5 mol% Ce doped samples are about 12.9, 11.8, 11.1 and 10.5 nm, respectively, which indicates that cerium doping can effectively restrain grain growth. Moreover, comparing the Ce-doped In_2O_3 with pure In_2O_3, angle shifts were detected to the (440) and (622) peaks (shown in Fig. 2). This could be ascribed to the difference between the radii of In and Ce ions. The radius of an Ce ion is larger than that of In ion, (Ce^{4+}:0.92 Å, Ce^{3+}:103.4 Å, In^{3+}:0.81 Å). Therefore, the substitution of Ce ions for In ions induced the angle shift of diffraction peaks towards smaller angles, further confirming that Ce ions are incorporated into the In_2O_3 lattice.

The morphologies and microstructures of the obtained In_2O_3 can be observed from FESEM images (shown in Fig. 3a–d). All the samples exhibit flower- like structures. As seen from the SEM image of Fig. 3a, the undoped In_2O_3 samples exhibit homogenous hierarchical flower-like microspheres with the diameter of about 3 μm. The inset of Fig. 3a showed these flower-like hierarchical structures are composed of a lot of small nanosheets. For the doped samples, with the increase of doping amount, the average sizes of the flower-like spheres were also decrease, the boundaries of as-prepared In_2O_3 microstructures gradually become more and more unconspicuous, which probably resulted from suppressed grain boundary migration and increased the energy barrier for grain growth.

TEM and HRTEM were employed to further investigate the structural features of the Ce-doped In_2O_3 sample. Fig. 4a shows the TEM image of a 3.0 mol% Ce-doped In_2O_3 hierarchical flower-like microsphere. The inset of Fig. 4a is the selected area electron diffraction pattern, in which a series of diffraction rings can be clearly observed. It shows that these In_2O_3 microspheres are polycrystalline in nature. The high-magnification TEM (HMTEM; Fig. 4b) images the In_2O_3 microspheres are made up of numerous nanorods. The inseted patterns shows the average distance between adjacent lattice fringes is 0.292 nm, corrsponding to the (222) planes of cubic In_2O_3. On the whole, the In_2O_3 nanorods which aggregate into In_2O_3 building blocks are formed by nanocrystallites. The energy dispersive X-ray spectroscopic (EDS) elemental mapping images

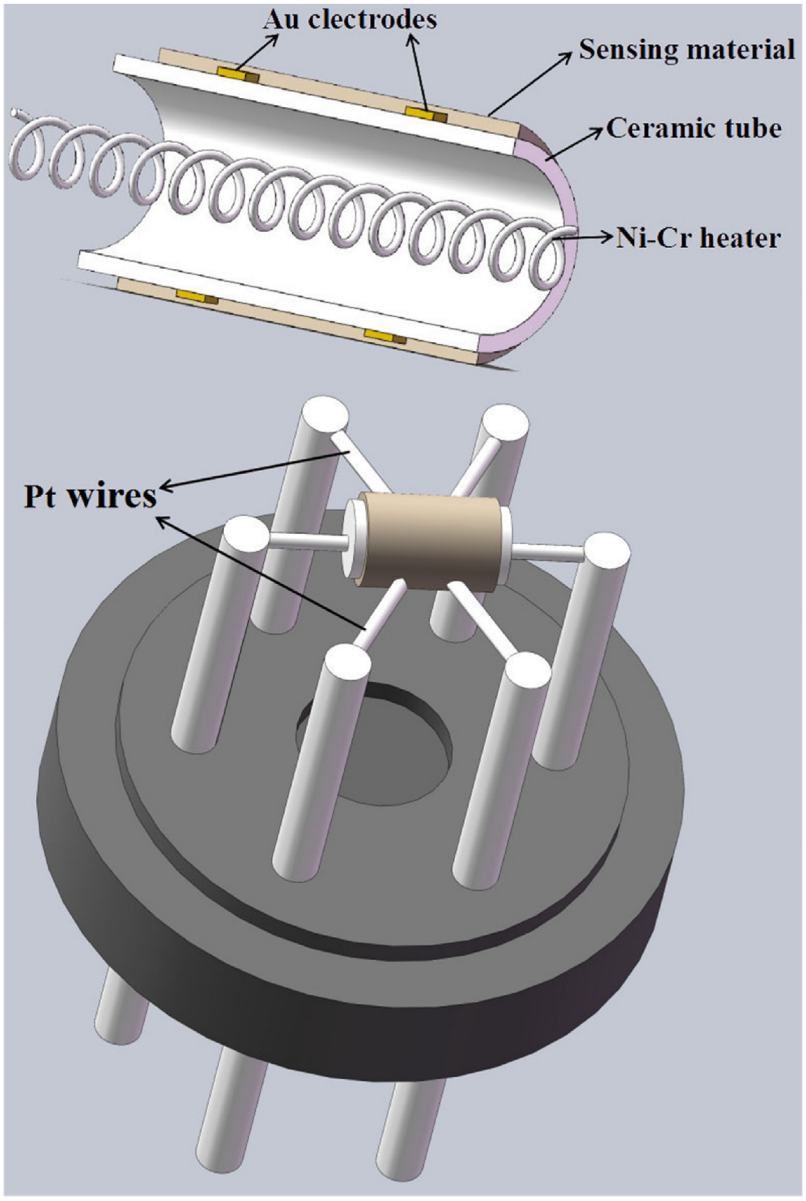

Fig 1. Schematic diagram of the gas sensor.

(Fig. 4c–e) confirms the composition of the product and the spatial distribution of the elements. Evidently, In and O signals were detected as a flower-like microspheres structure. And Ce signals were detected in the whole spherical region, which revealed the uniform distributions of Ce element over the whole hierarchical flower-like microspheres.

XPS (shown in Fig. 5a–d) was investigated to demonstrate the surface elemental compositions and their chemical status of the as prepared 3 mol% Ce-doped In_2O_3 microspheres. From its XPS survey spectrum (shown in Fig. 5a), the characteristic peaks of In, O, C, and Ce can be clearly observed. The adventitious carbon 1 s peak at 284.74 eV was used for calibration the binding energy. Fig. 5b–d show the high resolution scans of In 3d, Ce 3d, and O 1s, respectively. The In 3d spectrum (shown in Fig. 5b) has two strong peaks at binding energy of 444.50 and 452.18 eV. They can be respectively indexed to the characteristic spin-orbit split states of In $3d_{5/2}$ and In $3d_{3/2}$, indicating a In oxidation state of +3. The XPS spectrum of Ce 3d electrons (displayed in Fig. 5c) can be devided into several Gaussian peaks). In this figure, the peaks at 881.97, 883.02, 887.89, 900.79, 907.52 and 916.49 eV are attributed to Ce^{4+}, while 884.62, 898.24 and 903.53 eV are the characteristic peaks of Ce^{3+} ions. This confirms that Ce^{4+} and Ce^{3+} coexist in the lattice. The content of Ce^{4+} (1.512%) was higher than that of Ce^{3+} (0.728%). The O 1s peak is asymmetric and could be fitted into three Gaussian components located at 529.94, 530.60 and 531.94 eV in Fig. 5d. respectively. The Ol component is attributed to the lattice oxygen species, the middle of the three peaks was Ov component is associated with oxygen vacancy and the Oc is ascribed to chemisorbed oxygen in the surface of In_2O_3. The analysis result about O 1 s spectrum for pure In_2O_3 is similar without marked difference.

3.2. Gas-sensing properties

In order to illuminate that the doping of Ce into In_2O_3 microstructures is an effective way to improve the device of the In_2O_3-based gas sensor, the gas sensing characteristics of the sensors based on pure and Ce doped amounts of In_2O_3 flower-like microspheres were evaluated to illuminate the effect of Ce dop-

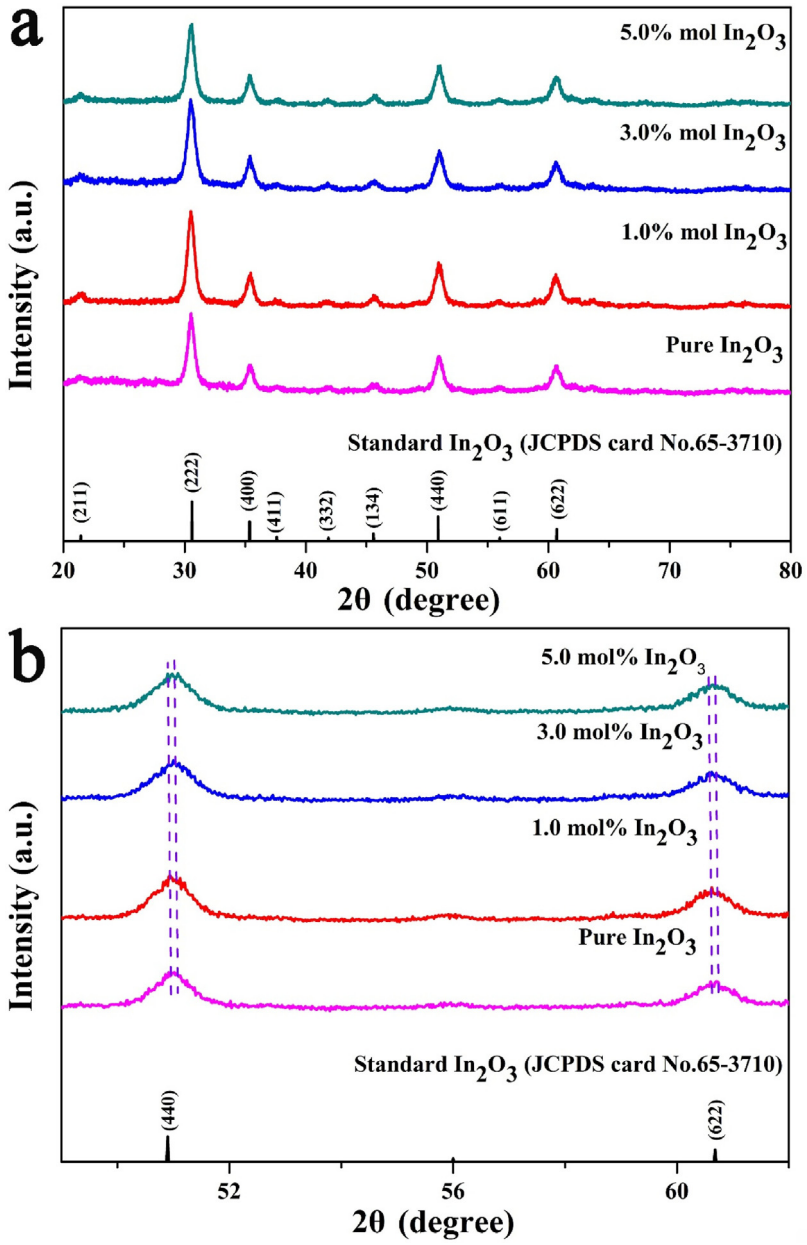

Fig. 2. (a) XRD patterns of flower-like Ce-doped In_2O_3 microspheres with different molar ratios, (b) Comparison of (440) and (622) peaks from XRD patterns.

ing. The operating temperature and the amount of doping play important roles in the gas sensing properties for metal oxide semiconductor gas sensor. Fig. 6a shows their gas response to 100 ppm acetone measured at different operating temperatures. For all the samples, the responses of the sensors initially increase with the operating temperature, which may attribute to the gas molecule could overcome the activation energy barrier of the surface reaction with the increased temperature. Obviously, all samples have a common optimum operating temperature at 250 °C. After the maximal response value, the response decreased with ulteriorly increasing the operating temperature. The major cause might be that the adsorption ability of target gas molecules was lower than that of desorption at high temperature, which resulted in reduced amounts of test molecules involved in the surface reaction. Furthermore, the sensing performances of all the samples are compared. The sensor based on the pure In_2O_3 has a maximum sensitivity of 6.3–100 ppm acetone, while the sensors based on the Ce-doped In_2O_3 showed greatly enhanced responses of 17.8, 27.5, and 22.6 for the Ce doping amounts of 1.0 mol%, 3.0 mol%, and 5.0 mol%, respectively. Thus, 3.0 mol% Ce-doped In_2O_3 exhibited the highest response to 100 ppm acetone, 4.3 times higher than that of the undoped In_2O_3. The particular reasons for it could be clarified as following. XRD patterns indicated Ce ions could enter In_2O_3 lattice. But as suggested by Noboru Yamazoe's work [45], in addition to the crystal lattices, Ce^{4+} ions are also prone to located at grain boundary because of the different ion valence states and ion radii between Ce^{4+} and In^{3+} ions, Therefore, Ce doping could effectively suppress the In_2O_3 grain growth and grain size decreased with the Ce^{4+} doping. In_2O_3 nanoparticals with small grain size could expose more sensitive sites, which was very helpful to improve the sensitivity. However, when the doping mount was large, the excess Ce ions could occupy the active sites on the surface of flower-like In_2O_3 microspheres, which is disadvantageous for the gas adsorption. Considering the above two effects, the highest response could be obtained at the optimum doping concentration of 3%.

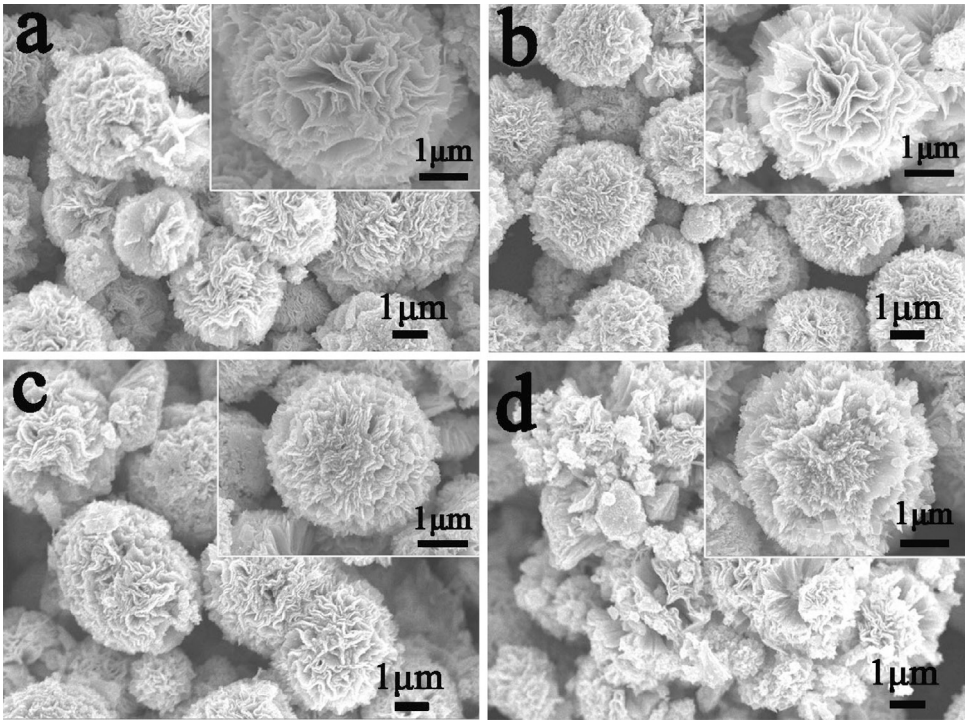

Fig. 3. FESEM images of (a) pure, (b) 1.0 mol%, (c) 3.0 mol%, (d) 5.0 mol% Ce-doped In_2O_3 hierarchical flower-like micrpspheres, the insets are high-magification images.

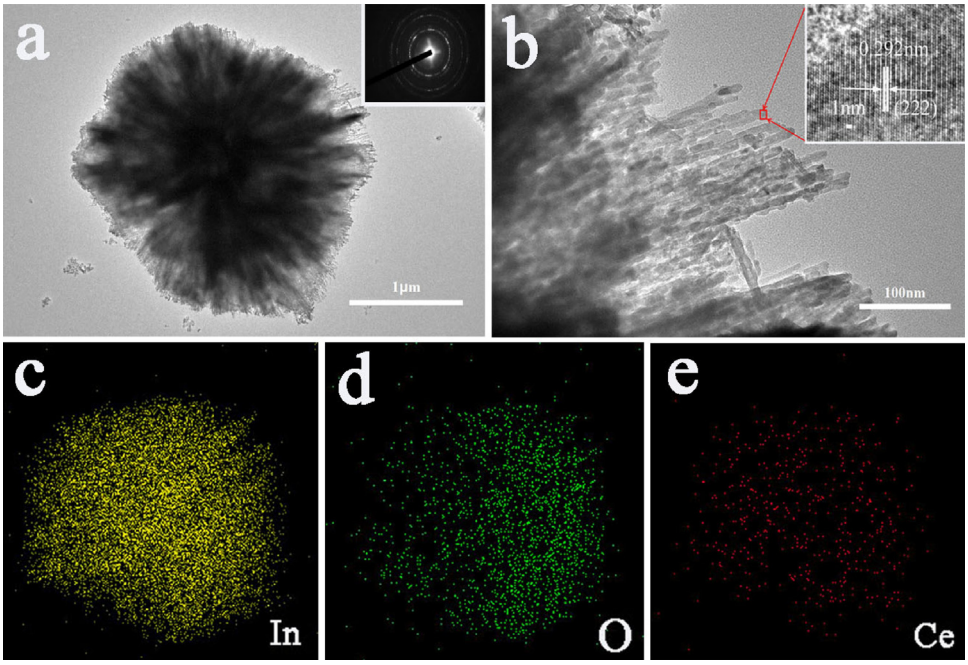

Fig. 4. (a) TEM images patterns of the 3.0 mol% Ce-doped In_2O_3 samples. The insets are selected area election diffraction (SAED) patterns. And (b) is the HRTEM images of selected areas. (c)–(e) are EDS elemental maps.

The responses of pure In_2O_3 and 3 mol% Ce-doped In_2O_3 under different concentrations of acetone from 10 to 1000 ppm at 250 °C were revealed in Fig. 6b. Obviously, the Ce doped sample has higher sensitivity than the undoped one. Moreover, the responses are almost linearly proportional to the gas concentration in the range from 10 ppm to 200 ppm for these two sensors. At higher gas concentration, the responds are almost saturated, implying that nearly all the active sites take part in the surface reaction. Interestingly, the saturation concentrations of detected target gas are almost the same. It is deduced that these two samples have the same amounts of active sites for the surfaces. This is consisted with the XPS results about O 1s spectrum.

Subsequently, the gas response of pure and 3 mol% Ce-doped In_2O_3 sensors to a wide range of VOCs were tested at 250 °C. Fig. 6c plots their sensitivities to eight kinds of gases, including acetone, ethanol, isopropanol, methanol, formaldehyde, xylene, toluene and benzene. As shown in Fig. 6c, the 3 mol% Ce-doped In_2O_3 samples display enhanced responses for most target gases compared

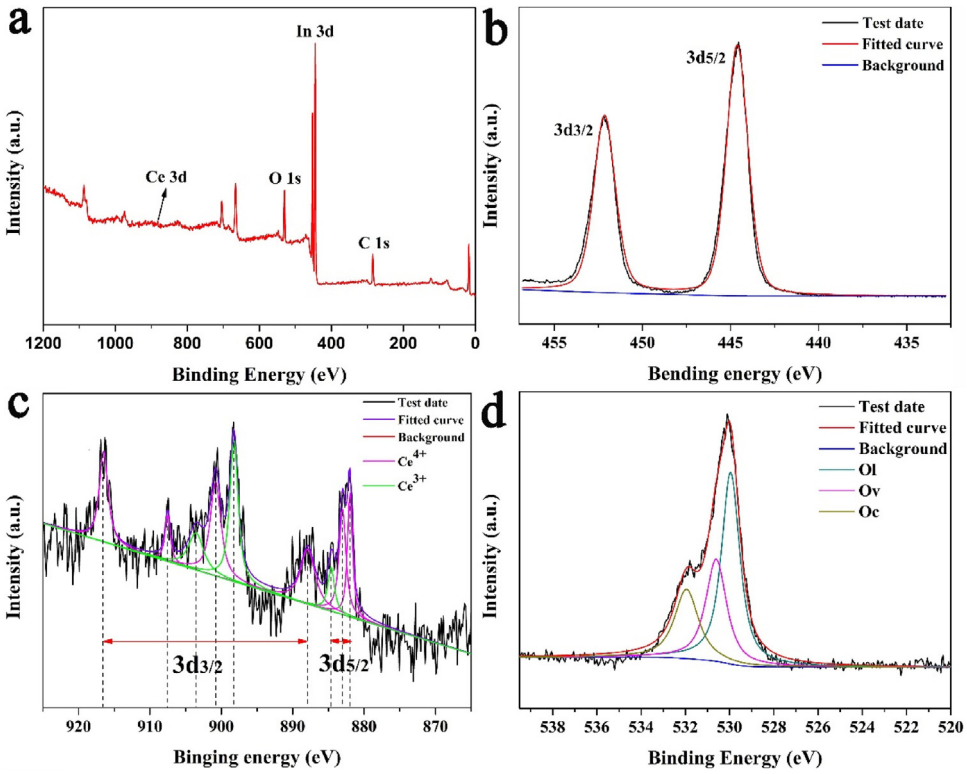

Fig. 5. XPS spectra of the 3.0 mol% Ce-doped In_2O_3 hierarchical flower-like microspheres: (a) a survey scan, (b) In 3d, (c) Ce 3d, (d) O 1s.

to the pure In_2O_3. Moreover, its response to 200 ppm acetone is the highest (Ra/Rg = 41.8), 4.3 times higher than that of pure In_2O_3 to acetone.

The response-recovery behavior is also a crucial characteristic in a rea-time gas monitoring process. The response and recovery transients of the sensor based on pure and 3.0 mol% Ce-doped In_2O_3 to 200 ppm acetone at the optimal operating temperature of 250 °C are presented in Fig. 7a. It is fairly visualized that the response time and recovery time of the sensor based on the 3.0 mol% Ce-doped sample were shorter than the undoped sample. The response and recovery times of 3.0 mol% are about 2 and 154 s, respectively, the counterparts for undoped sample is 5 and 182s. Hence, Ce doping can speed up the response and recovery rate. This has been confirmed by Song's work, which studied acetone sensing properties of Ce-doped SnO_2 hollow spheres [46]. The response was also detected for four reversible cycles, which is shown in Fig. 7b. There is no clear floating in responses during the periods of cycle measurement to 200 ppm acetone at 250 °C, indicating its good repeatability and stability of the 3 mol% Ce-doped In_2O_3 sensor. Its long term stability of 3 mol% Ce-doped In_2O_3 sensor to 200 ppm acetone was tested under the optimum conditions for one month. As shown in Fig. 7c, the response values just fluctuated 5% around 41.8. Therefore, an excellent stability of acetone sensors based on Ce-doped In_2O_3 flower-like microspheres could be obtained and its eminent gas sensing characteristic might make it particularly attractive as a promising practical sensor.

3.3. Mechanism of the enhanced gas sensing performance

The sensing mechanism of metal oxides gas sensors has been clarified in previous works [47,48]. The most widely accepted theory is based on the change in the electrical conductivity caused by the interactions between the surface chemisorbed oxygen species and target gases. It is well known that indium oxide is a typical *n*-type metal oxide semiconductor. When the sensor is exposed to air, a large number of oxygen molecules can be adsorbed on the In_2O_3 surface, then may capture free electrons from the conduction band to form chemisorbed oxygen ions, such as O_2^-,O^-, O^{2-}. Meanwhile, the formed depleting layer on the surface of the sensing materials results in the increased material resistance. The decrease of the electron concentration in the conduction band leads to high resistance. This progress can be expressed as the following reactions:

$$O_{2(gas)} \rightarrow O_{2(ads)} \quad (1)$$

$$O_{2(ads)} + e^- \rightarrow O^-_{2(ads)} \quad (2)$$

$$O^-_{2(ads)} + e^- \rightarrow 2O^-_{(ads)} \quad (3)$$

$$O^-_{(ads)} + e^- \rightarrow O^{2-}_{(ads)} \quad (4)$$

When reducing gas (e.g. acetone) is present, they can react with the chemisorbed oxygen ions absorbed on the In_2O_3 surface and release the trapped electrons back to the conduction band of In_2O_3, resulting in the decrease in the sensor resistance [49]. The reaction process is as follows:

$$CH_3COCH_3 + 8O^-_{(ads)} \rightarrow 3CO_2 + 3H_2O + 8e^- \quad (5)$$

The enhancement of the gas response of the sensor based on the Ce-doped In_2O_3 hierarchical flower-like microspheres are likely to be attribute to the changes in crystallite size, carrier concentration and specific surface area. The above results of XRD, Ce doping leads to a decrease in the average grain size, Small grain size means that large specific surface area, more active sites for surface reaction and large response The carrier concentration maybe another key factor for the improved sensitivity. According to the research of Kim ea. al [50], the gas response can be written as follows:

$$S_a = \frac{R_a}{R_g} = \frac{n_g}{n_a} = \frac{n_a + \nabla n}{n_a} = 1 + \frac{\nabla n}{n_a} \quad (6)$$

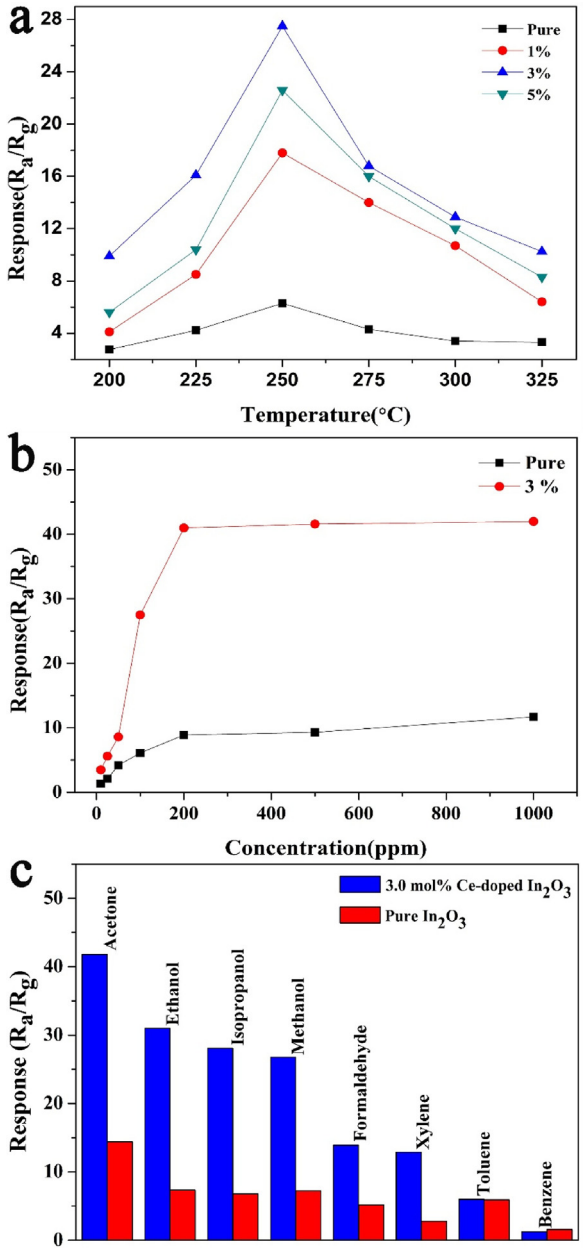

Fig. 6. (a) Response of sensors bases on pure, 1.0 mol%, 3.0 mol% and 5.0 mol% Ce-doped In_2O_3 to 100 ppm acetone as function of the operating temperature. (b) Response of sensors bases on pure and 3.0 mol% Ce-doped In_2O_3 samples toward acetone at different concentrations. (c) Comparison in the response of pure and 3.0 mol% Ce-doped In_2O_3 samples to 200 ppm different test gases at 250 °C.

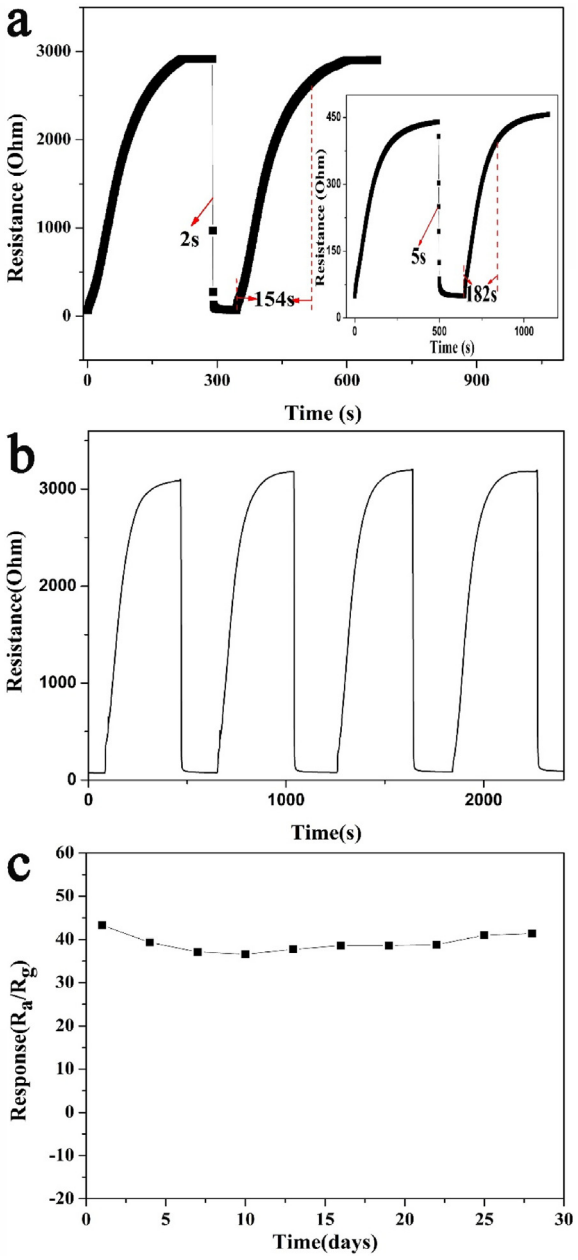

Fig. 7. (a) Response and recovery curves of 3.0 mol Ce-doped In_2O_3 samples, (b) four reversible cycles and (c) The long-term stability of 3.0 mol% Ce-doped In_2O_3 samples to 200 ppm acetone at 250 °C.

Where Ra and Rg are the resistances in air and target gas, n_g and n_a are the electron concentration in target gas and air and $\nabla n = n_g - n_a$ is the variation of electron concentration when exposed to target gas. Our result showed that the resistance of Ce doping samples was larger than that of the pure In_2O_3. For example, the resistances of pure and 3.0 mol% Ce-doped In_2O_3 are 450 ohm and 3000 ohm, respectively. It could be attributed to two reasons. First, one Ce^{4+} ion can capture one electron and convert into Ce^{3+}, which reduces the electron concentration. Second, Ce^{4+} with the large radius may change the energy structure, resulting in the lowered carrier amount. From Eq. (6), the lower electronic concentration is, the higher sensitivity for the reducing gas can be. The increased resistance in the Ce doped In_2O_3 is helpful to improve the respond for the acetone. The hierarchical morphologies of gas sensor may play a significant role in improving the gas sensor properties due to the abundant framework of gas diffusion and the chemical absorption as well as reaction on the surface of the In_2O_3 [51]. In this work, the hierarchical structure of In_2O_3 nanostructures with excellent porosity structure and large specific surface area enhance the diffusion of acetone and offer abundant active sites for chemisorption and reactions of acetone, which leaded to accelerate diffusion rate of acetone vapour and faster response and recovery speed. The more detailed reason and qualitative explanation need further investigation.

4. Conclusion

In summary, we successfully synthesized the pure and Ce-doped flower-like In_2O_3 with well-dispersed hierarchical microstructures and uniform sizes by the facile hydrothermal route. The results of gas sensing measurement indicated that the sensor based on

the 3.0 mol% Ce-doped In_2O_3 has the significantly enhanced gas response to acetone compared with that of the undoped, 1.0 mol%, and 5.0 mol% Ce-doped In_2O_3. The changes in crystallite size, carrier concentration and specific surface area caused by Ce doping could be responsible for the improvement of the sensing properties. Hence, we can confirm that the doping of Ce-doped hierarchical flower-like In_2O_3 microspheres is a promising strategy for improving the gas sensing performance of the In_2O_3-based gas sensor.

Acknowledgements

This work is supported by National Nature Science Foundation of China (Nos. 61573164, 61520106003, 61327804), National High-Tech Research and Development Program of China (863 Program, No. 2014AA06A505).

References

[1] S.-W. Choi, A. Katoch, J.H. Kim, S.S. Kim, Prominent reducing gas-sensing performances of n-SnO_2 nanowires by local creation of p-n heterojunctions by functionalization with p-Cr_2O_3 nanoparticles, ACS Appl. Mater. Interfaces 6 (2014) 17723–17729.
[2] J.Y. Liu, M.J. Dai, T.S. Wang, P. Sun, Enhanced gas sensing properties of SnO_2 hollow spheres decoratedwith CeO_2 nanoparticles heterostructure composite materials, ACS Appl. Mater. Interfaces 8 (2016) 6669–6677.
[3] H.H. Yan, P. Song, S. Zhang, Z.X. Yang, Q. Wang, Dispersed SnO_2 nanoparticles on MoS_2 nanosheets for superior gas-sensing performances to ethanol, RSC Adv. 5 (2015) 79593–79599.
[4] M. Bao, Y.J. Chen, F. Li, J.M. Ma, T. Lv, Y.J. Tang, L.B. Chen, Plate-like p–n heterogeneous NiO/WO_3 nanocomposites for high performance room temperature NO_2 sensors, Nanoscale 6 (6) (2014) 4063–4066.
[5] V. Kruefu, A. Wisitsoraat, A. Tuantranont, S. Phanichphant, Ultra-sensitive H_2S sensors based on hydrothermal/impregnation-made Ru-functionalized WO_3 nanorods, Sens. Actuators, B 215 (2015) 630–636.
[6] C. Liu, B.Q. Wang, T. Liu, P. Sun, Facile synthesis and gas sensing properties of the flower-like NiO-decorated ZnO microstructures, Sens. Actuators, B 235 (2016) 294–301.
[7] S.M. Wang, J. Cao, W. Cui, X.F. Li, D.J. Li, Facile synthesis and excellent formaldehyde gas sensing properties of novel spindle-like In_2O_3 porous polyhedral, Sens. Actuators, B 237 (2016) 944–952.
[8] K. Anand, J. Kaur, R.C. Singh, R. Thangaraj, Effect of terbium doping on structural, optical and gas sensingproperties of In_2O_3 nanoparticles, Mater. Sci. 39 (2015) 476–483.
[9] X. Li, C. Wang, X. Zhou, J. Liu, P. Sun, G. Lu, Gas sensing properties of flower-like ZnO prepared by a microwave-assisted technique, RSC Adv. 4 (2014) 47319–47324.
[10] X. Jia, H. Fan, M. Afzaal, X. Wu, P. O'Brien, Solid state synthesis of tin-doped ZnO at room temperature: characterization and its enhanced gas sensing and photocatalytic properties, J. Hazard. Mater. 193 (2011) 194–199.
[11] R.G. Pavelko, M. Yuasa, T. Kida, K. Shimanoe, N. Yamazoe, Impurity level inSnO_2 materials and its impact on gas sensing properties, Sens. Actuators, B 210 (2015) 719–725.
[12] P. Sun, X. Mei, Y. Cai, J. Ma, Y. Sun, X. Liang, F. Liu, G. Lu, Synthesis and gas sensing properties of hierarchical SnO_2 nanostructures, Sens. Actuators, B 187 (2013) 301–307.
[13] B. Liu, H.Q. Yang, H. Zhao, L.J. An, L.H. Zhang, R.Y. Shi, L. Wang, L. Bao, Y. Chen, Synthesis and enhanced gas-sensing properties of untralong NiOnanowires assembled with NiO nanocrystals, Sens. Actuators, B: Chem. 156 (2011) 251–262.
[14] J.S. Cho, J.M. Won, J.H. Lee, Y.C. Kang, Synthesis and electrochemical properties of spherical and hollow-structured NiO aggregates created by combining the Kirkendall effect and Ostwald ripening, Nanoscale 7 (2015) 19620–19626.
[15] J.S. Cho, Y.J. Hong, J.H. Lee, Y.C. Kang, Design and synthesis of micron-sized spherical aggregates composed of hollow Fe_2O_3 nanospheres for use in lithium-ion batteries, Nanoscale 7 (2015) 8361–8367.
[16] X. Hu, J.C. Yu, J. Gong, Q. Li, G. Li, α-Fe_2O_3 nanorings prepared by a microwave assisted hydrothermal process and their sensing properties, Adv. Mater. 19 (2007) 2324–2329.
[17] C. Wang, R.Z. Sun, X. Li, Y.F. Sun, P. Sun, F.M. Liu, G.Y. Lu, Hierarchical flowerlike WO_3 nanostructures and their gas sensing properties, Sens. Actuators, B: Chem. 204 (2014) 224–230.
[18] D.L. Chen, L.F. Ge, L. Yin, H.Y. Shi, D.W. Yang, J. Yang, R. Zhang, G.S. Shao, Solvent-regulated solvothermal synthesis and morphology-dependent gas sensing performance of low-dimensional tungsten oxide nanocrystals, Sens. Actuators, B: Chem. 205 (2014) 391–400.
[19] D. Han, P. Song, S. Zhang, H.H. Zhang, Enhanced methanol gas-sensing performance of Ce-doped In_2O_3 porous nanospheres prepared by hydrothermal method, Sens. Actuators, B 216 (2015) 488–496.
[20] S. Zhang, P. Song, H.H. Yan, Q. Wang, Self-assembled hierarchical Au-loaded In_2O_3 hollow microspheres with superior ethanol sensing properties, Sens. Actuators, B 231 (2016) 245–255.
[21] S. Zhang, P. Song, J. Li, J. Zhang, Z.X. Yang, Q. Wang, Facile approach to prepare hierarchical Au-loaded In_2O_3 porous nanocubes and their enhanced sensing performance towards formaldehyde, Sens. Actuators, B 241 (2017) 1130–1138.
[22] P. Sun, X. Mei, Y. Cai, J. Ma, Y. Sun, X. Liang, et al., Synthesis and gas sensing properties of hierarchical SnO_2 nanostructures, Sens. Actuators, B-Chem 187 (2013) 301–307.
[23] B.X. Xiao, F. Wang, C.B. Zhai, P. Wang, C.H. Xiao, Facile synthesis of In_2O_3 nanoparticles for sensing properties at low detection temperature, Sens. Actuators, B 235 (2016) 251–257.
[24] C. Li, D.H. Zhang, S. Han, X.L. Liu, T. Tang, C.W. Zhou, Diameter-controlledgrowth of single-crystalline In_2O_3 nanowires and their electronic properties, Adv. Mater. 15 (2003) 143–146.
[25] Z.X. Cheng, X.B. Dong, Q.Y. Pan, J.C. Zhang, X.W. Dong, Preparation and characterization of In_2O_3 nanorods, Mater. Lett. 60 (2006) 3137–3140.
[26] R.A. Ismail, O.A. Abdulrazaq, K.Z. Yahya, Preparation and characterization of In_2O_3 thin films for optoelectronic applications, Surf. Rev. Lett. 12 (2005) 515–518.
[27] R. Sharma, S. Mane Rajaram, S.K. Min, S.H. Han, Optimization of growth ofIn_2O_3 nano-spheres thin films by electrodeposition for dye-sensitized solar cells, J. Alloys Compd. 479 (2009) 840–843.
[28] Z.Q. Li, H.-F. Fei, Y.X. Tan, X.Z. Zhang, Synthesis and characterization of self-assembled three-dimensional flower-like iron(III) oxide?indium(III) oxide binary nanocomposites, RSC Adv. 5 (2015) 38093–38099.
[29] L.P. Gao, Z.X. Cheng, Q. Xiang, Y. Zhang, J.Q. Xu, Porous corundum-type In_2O_3 nanosheets: synthesis and NO_2 sensing properties, Sens. Actuators, B 208 (2015) 436–443.
[30] Q.S. Liu, W.G. Lu, A.H. Ma, J.K. Tang, J. Lin, J.Y. Fang, Study of quasi-monodisperseln$_2O_3$ nanocrystals: synthesis and optical determination, J. Am. Chem. Soc. 127 (2005) 5276–5277.
[31] C.Q. Wang, D. Chen, X.L. Jiao, C.L. Chen, Lotus-root-like In_2O_3 nanostructures: fabrication, characterization, and photoluminescence properties, J. Phys. Chem. C 111 (2007) 13398–13403.
[32] X.P. Shen, H.J. Liu, X. Fan, Y. Jiang, J.M. Hong, Construction and photoluminescence of In_2O_3 nanotube array by CVD-template method, J. Cryst. Growth 276 (2005) 471–477.
[33] Y.F. Hao, G.W. Meng, C.H. Ye, L.D. Zhang, Controlled synthesis of In_2O_3 octahedrons and nanowires, Cryst. Growth Des. 5 (2005) 1617–1621.
[34] A. Qurashi, E.M. El-Maghraby, T. Yamazaki, T. Kikuta, Catalyst-free shape controlled synthesis of In_2O_3 pyramids and octahedron: structural properties and growth mechanism, J. Alloys Compd. 480 (2009) 9–12.
[35] T. Hyodo, H. Inoue, H. Motomur, K. Matsuo, T. Hashishin, J. Tamaki, Y. Shimizu, M. Egashira, NO_2sensing properties of macroporous In_2O_3-basedpowders fabricated by utilizing ultrasonic spray pyrolysis employing poly methylmethacrylate microspheres as a template, Sen. Actuators, B: Chem. 151 (2010) 265–273.
[36] X.M. Xu, P.L. Zhao, D.W. Wang, P. Sun, L. You, Preparation and gas sensing properties of hierarchical flower-like In_2O_3 microspheres, Sens. Actuators, B 176 (2013) 405–412.
[37] X.M. Xu, H.J. Zhang, X.L. Hu, P. Sun, Y.S. Zhu, Hierarchical nanorod-flowers indium oxide microspheres and their gas sensing properties, Sens. Actuators, B 227 (2016) 547–553.
[38] C. Wang, X.B. Cui, J.Y. Liu, X. Zhou, X.Y. Cheng, P. Sun, Design of superior ethanol gas sensor based on al-doped NiO nanorod-flowers, ACS Sens. 1 (2016) 131–136.
[39] J. Zhao, T.L. Yang, Y.P. Liu, Z.Y. Wang, X.W. Li, Enhancement of NO_2 gas sensing response based on ordered mesoporous Fe-doped In_2O_3, Sens. Actuators, B 191 (2014) 806–812.
[40] X.L. Hu, L.Y. Tian, H.B. Sun, B. Wang, Y. Gao, Highly enhanced NO_2 sensing performances of Cu-doped In_2O_3 hierarchical flowers, Sens. Actuators, B 221 (2015) 297–304.
[41] Y. Qu, H. Wang, H. Chen, J. Xiao, Z.D. Lin, K. Dai, Highly sensitive and selective toluene sensor based on Ce-doped coral-like SnO_2, RSC Adv. 5 (2015) 16446–16449.
[42] G.X. Wan, S.Y. Ma, X.B. Li, F.M. Li, H.Q. Bian, L.P. Zhang, W.Q. Li, Synthesis and acetone sensing properties of Ce-doped ZnO nanofibers, Mater. Lett. 114 (2014) 103–106.
[43] Z.W. Jiang, Z. Guo, B. Sun, Y. Jia, Highly sensitive and selective butanone sensors based on cerium-doped SnO_2 thin films, Sens. Actuators, B 145 (2010) 667–673.
[44] X.W. Li, P. Sun, T.L. Yang, J. Zhao, Z.Y. Wang, W.N. Wang, Y.P. Liu, G.Y. Lu, Template-free microwave-assisted synthesis of ZnO hollow microspheres and their application in gas sensing, CrystEngComm 15 (2013) 2949–2955.
[45] N. Yamazoe, G. Sakai, K. Shimanoe, Oxide semicomductor gas sensors, Catal. Surv. Asia 7 (2003) 63–75.
[46] P. Song, Q. Wang, Z.X. Yang, Preparation, characterization and acetone sensing properties of Ce-doped SnO_2hollow spheres, Sens. Actuators, B 173 (2012) 839–846.
[47] P. Sun, X. Zhou, C. Wang, B. Wang, X.M. Xu, One-step synthesis and gas sensing properties of hierarchical Cd-doped SnO_2 nanostructures, Sens. Actuators, B 190 (2014) 32–39.

[48] P. Sun, C. Wang, X. Zhou, P.F. Cheng, Cu-doped $-Fe_2O_3$ hierarchical microcubes: synthesis and gas sensing properties, Sens. Actuators, B 193 (2014) 616–622.
[49] L.P. Gao, F.M. Ren, Z.X. Cheng, Y. Zhang, Q. Xiang, J.Q. Xu, Porous corundum-type In_2O_3 nanoflowers: controllable synthesis, enhanced ethanol-sensing properties and response mechanism, CrystEngComm 17 (2015) 3268–3276.
[50] H.J. Kim, Kwon-Il Choi, Kang-Min Kim, Highly sensitive C_2H_5OH sensors using Fe-doped NiO hollow spheres, Sens. Actuators, B 171-172 (2012) 1029–1037.
[51] C.H. Zhao, B.Y. Huang, E.Q. Xie, Improving gas-sensing properties of electrospun In_2O_3 nanotubes by Mg acceptor doping, Sens. Actuators, B 207 (2015) 313–320.

Biographies

Dongdong Wei received the BS degree in Changchun University of Science and Technology in 2016. He is currently studying for his MS degree in College of Electronic Science and Engineering, Jilin University, China. His research interests include the synthesis of functional materials and their applications in gas sensors.

Zhangshu Huang received the BS degree in Department of Electronic Science and Engineering in 2015. He is currently studying for his MS degree in College of Electronic Science and Engineering, Jilin University, China.

Liwei Wang received the BS degree in Changchun University of Science and Technology in 2014. He is currently studying for his MS degree in College of Electronic Science and Engineering, Jilin University, China.

Xiaohong Chuai received the Ph. D degree in inorganic nonmetal science from Beijing University of science in 2001, and then worked at the school of Electronic Science and engineering, Jilin University. Now, she is engaged in the synthesis and characterization of the semiconducting functional materials and gas sensors.

Sumei Zhang obtained her PhD from Jilin University of China in 2005. Presently, she is working as associate professor in Electronics Science and Engineering department of Jilin University. Her current research interests are nanoscience and gas sensors.

Geyu Lu received the BS degree in electronic sciences in 1985 and the MS degree in 1988 from Jilin University in China and the Dr Eng degree in 1998 from Kyushu University in Japan. Now he is a professor of Jilin University, China. Now, he is interested in the development of functional materials and chemical sensors received the B. Eng. Degree in Department of Electronic Science and Technology in 2004. He received his Doctor's degree in College of Electronic Science and Engineering at Jilin University in 2009. Now he is a lecturer of Jilin University, China. His current research is solid electrolyte gas sensor.